

Generalist Large Language Models for Molecular Property Prediction: Distilling Knowledge from Specialist Models

Khiem Le¹, Sreejata Dey¹, Marcos Martínez Galindo², Vanessa Lopez²,
Ting Hua¹, Nitesh V. Chawla¹, Hoang Thanh Lam²

¹ University of Notre Dame, IN, USA ² IBM Research

✉: t.l.hoang@ie.ibm.com

Abstract

Molecular Property Prediction (MPP) is a central task in drug discovery. While Large Language Models (LLMs) show promise as generalist models for MPP, their current performance remains below the threshold for practical adoption. We propose TreeKD, a novel knowledge distillation method that transfers complementary knowledge from tree-based specialist models into LLMs. Our approach trains specialist decision trees on functional group features, then verbalizes their learned predictive rules as natural language to enable rule-augmented context learning. This enables LLMs to leverage structural insights that are difficult to extract from SMILES strings alone. We further introduce rule-consistency, a test-time scaling technique inspired by bagging that ensembles predictions across diverse rules from a Random Forest. Experiments on 22 ADMET properties from the TDC benchmark demonstrate that TreeKD substantially improves LLM performance, narrowing the gap with SOTA specialist models and advancing toward practical generalist models for molecular property prediction.

1 Introduction

Molecular Property Prediction (MPP) plays a crucial role in the Drug Discovery (Wu et al., 2018; Liyaqat et al., 2025), aiming to predict the quantitative characteristics of drug candidates such as ADMET properties (Absorption, Distribution, Metabolism, Excretion, and Toxicity) (Ferreira and Andricopulo, 2019). Accurate prediction enables reliable screening of potential drug candidates at early stages, lowering experimental costs and optimizing efficiency. While traditional specialist models achieve strong performance on individual properties, they lack the ability to interact via natural language, provide explanations, or engage in scientific conversations (Chaves et al., 2024; Wang et al., 2025; Xia et al., 2025). Recently, the success of Large Language Models (LLMs) (Achiam

et al., 2023; Comanici et al., 2025) across diverse text-based tasks (Hendrycks et al., 2021; Suzgun et al., 2023) has motivated increasing efforts to develop LLM-based generalist models that can predict multiple properties while offering these interactive capabilities (Zhang et al., 2025). However, despite training LLMs on the textual modality of molecules (SMILES notation), their current performance on MPP remains far below that of specialist models, limiting their practical adoption for MPP (Guo et al., 2023; Zhong et al., 2024).

A key reason for this performance gap is that LLMs struggle to recognize functional groups (FGs), the substructures within a molecule that largely determine its properties (Andrews et al., 1984), when provided only SMILES strings (Castro Nascimento and Pimentel, 2023; Runcie et al., 2025). To address this limitation, several methods have been proposed that integrate additional structural modalities, such as 2D/3D graphs and fingerprints, into LLMs (Liu et al., 2023; Li et al., 2024; Le et al., 2024; Cao et al., 2025). However, these methods require a large-scale dataset, a complex adaptor, and an extra pretraining phase to align these modalities with LLMs (Li et al., 2023). This alignment process is resource-intensive and increases the risk of data leakage. Furthermore, LLMs have been shown to have difficulty in capturing the concept of property cliffs (Xia et al., 2023), which means situations where small changes in the structure of a molecule lead to significant changes in its properties (Maggiora, 2006; Stumpfe and Bajorath, 2012). In contrast, traditional tree-based specialist models have been proven to learn differently from crafted features and are better at capturing this concept (Xia et al., 2023).

In this work, we propose TreeKD, a novel knowledge distillation method that improves LLM performance on MPP by transferring complementary knowledge from tree-based specialist models. Instead of forcing LLMs to recognize FGs implic-

itly, we extract and provide all FGs found in each molecule (from a library of 40K), reducing the semantic gap between SMILES strings and natural language (Wellawatte and Schwaller, 2025). Building on the extracted features, we train a specialist decision tree for each property. Decision trees learn from crafted features differently than LLMs and are more sensitive to property cliffs, with their knowledge encoded in learned predictive rules. We then verbalize these rules as natural language and integrate them into the training context, enabling knowledge transfer from decision trees to LLMs.

To further enhance performance, we introduce rule-consistency, a test-time scaling technique inspired by bootstrap aggregating (Breiman, 1996). Instead of using a single decision tree, we train a Random Forest of N decision trees for each property and incorporate one randomly selected predictive rule into each training example. The randomness mirrors the inherent diversity in ensemble methods, preventing the LLM from over-relying on any single rule. At inference, rule-consistency ensembles N predictions from N different prompts, each augmented with a different predictive rule from the Random Forest, unlike self-consistency (Wang et al., 2023) which ensembles predictions from the same prompt.

Our main contributions are summarized as follows: 1) We propose TreeKD, a knowledge distillation approach that transfers complementary knowledge from tree-based specialist models to LLMs by verbalizing decision tree rules and integrating them into the training context. 2) We introduce rule-consistency, a test-time scaling technique that leverages Random Forest diversity to ensemble predictions across different rules, providing more robust predictions than sampling-based approaches. 3) Through extensive experiments on 22 ADMET properties from the TDC benchmark using Gemma-2-2B and Granite-3.3-2B, we demonstrate that TreeKD significantly improves over baseline LLMs on MPP, achieving competitive performance with specialist models while retaining the interpretability and natural language interaction capabilities unique to LLM-based methods.

2 Related Work

Generalist LLMs for MPP. A major practice in developing generalist models for MPP based on LLMs is curating a massive instruction dataset to train LLMs on (Zhang et al., 2025). Fang et al.

(2024) introduce Mol-Instructions, a dataset of 2M samples stemming from various sources such as PubChem and MoleculeNet, and show that training LLMs on this dataset improves their performance. Similarly, Yu et al. (2024) create a larger dataset, SMolInstruct, which contains 3.3M samples, and establish LLaSMol models by fine-tuning LLMs on it. Beyond straightforward training, Liu et al. (2024); Wang et al. (2025) aim to unleash the In-context Learning (ICL) (Brown et al., 2020) power of LLMs during inference by employing Meta-ICL (Min et al., 2022) during training. In addition, Liu et al. (2023); Li et al. (2024); Le et al. (2024); Cao et al. (2025) propose methods to assist LLMs in perceiving structural information of molecules by integrating additional structural modalities, such as 2D/3D graphs and fingerprints, though these methods are resource-intensive and exacerbate data leakage risk. Our goal is to boost LLMs’ performance by leveraging knowledge from tree-based specialist models. This approach is complementary to existing methods and does not require additional modalities or complex alignment procedures.

Knowledge Distillation with LLMs. Knowledge Distillation (KD) (Hinton et al., 2015) is a widely used method to train a neural network model (student) with the knowledge of another neural network model (teacher). Originally, this is done by minimizing the Kullback–Leibler (KL) divergence between their logit distributions. Then, Kim and Rush (2016) propose SeqKD as a variant of KD to train an LLM (student) with the knowledge of another LLM (teacher), minimizing the KL divergence between their next-token logit distributions. Notably, Alpaca (Taori et al., 2023; Chaudhary, 2023) and Vicuna (Chiang et al., 2023) are prominent examples of SeqKD. Recently, Gu et al. (2024); Yao et al. (2025) argue that reversing the KL divergence is more effective for SeqKD. Nevertheless, none of these methods enables training an LLM (student) with the knowledge of traditional tree-based models (teacher). Unlike traditional KD, which minimizes divergence between output distributions, our approach transfers knowledge by verbalizing decision tree rules as natural language and incorporating them into the training context.

3 Methodology

This section presents our proposed method, as illustrated in Figure 1. First, we extract functional groups (FGs) from molecules and train specialist

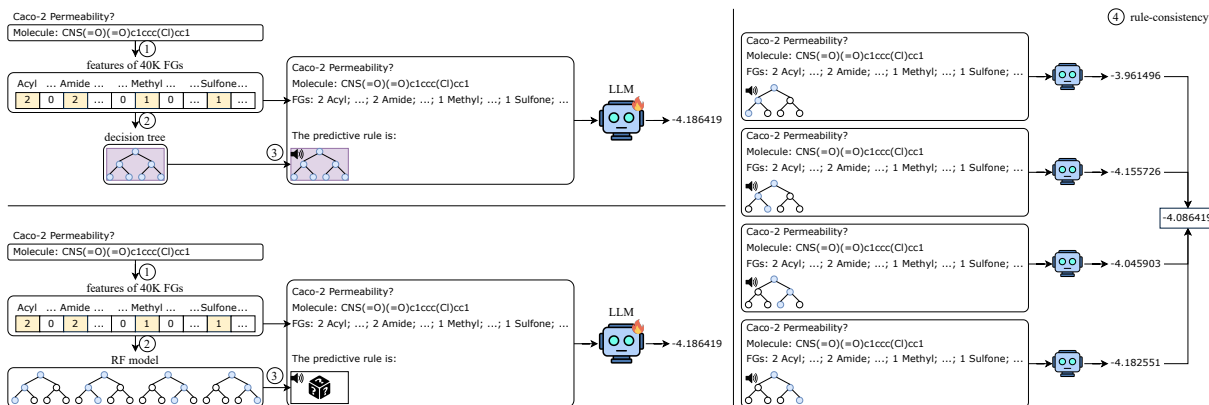


Figure 1: An overview of our proposed method TreeKD, consisting of the following four steps: ① Extract FGs, ② Construct Specialist Models, ③ Distill Knowledge from Specialist Models, and ④ Test-Time Scaling.

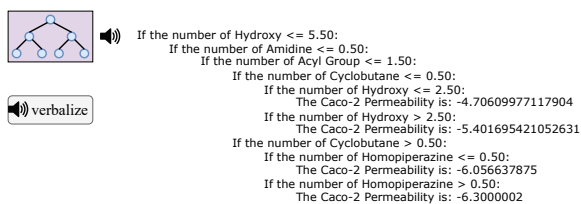


Figure 2: An example of verbalizing a predictive rule. The tree is turned into a hierarchy of if-then conditions, where indentation indicates the depth of nodes.

decision tree models on these features (Section 3.1). Then, we distill knowledge from the specialist models by verbalizing their predictive rules and incorporating them into training prompts (Section 3.2). Finally, we introduce rule-consistency, a test-time scaling technique that leverages diversity among decision trees in a Random Forest (Section 3.3).

3.1 Extract FGs and Construct Specialist Models

Functional groups (FGs) are specific sets of atoms within molecules that largely govern chemical reactivity and properties. We use FGs as interpretable features to train decision trees that yield human-readable predictive rules. These rules encode the relationship between FGs and target properties, serving as the knowledge to be distilled into LLMs.

Let P denote the set of properties under consideration. For each property $p \in P$ (e.g., Caco-2 Permeability), we define the training dataset of n_p samples as $D_p = \{(m_i, y_i)\}_{i=1}^{n_p}$, where m_i represents an input molecule as a SMILES string and y_i denotes its label. Given the input molecule m_i , we utilize SMART-Chemist (Gutermuth et al., 2025), which efficiently implements SMARTS pattern matching (Schmidt et al., 2019), to extract the most

common 40K FGs, forming a vector v_i of crafted features that indicates the occurrence frequency of 40K FGs in m_i . For each property $p \in P$, on the training dataset $D_p^{FGs} = \{(v_i, y_i)\}_{i=1}^{n_p}$, we then train a specialist decision tree r_p (see Figure 1 Top-Left). Note that the maximum depth of the decision tree is set to 6 to balance its performance and complexity. Detailed hyper-parameters of specialist models are provided in Appendix A.

3.2 Distill Knowledge from Specialist Models

Unlike traditional knowledge distillation that requires matching output distributions, we use natural language as a bridge to transfer knowledge from decision trees to LLMs. To train an LLM (student) with the knowledge of a decision tree (teacher), we exploit the tree’s learned predictive rule, which encodes the knowledge acquired during training. For each property $p \in P$ and the corresponding decision tree r_p , we verbalize its predictive rule. Specifically, we express the rule as text that the LLM can process by representing it as a hierarchy of if-then conditions. The structure of the hierarchy is indicated by the number of tab characters (`\t`) used for indentation. Figure 2 provides an example of how a predictive rule is converted into text. We then incorporate the verbalized rule into the prompt associated with the input molecule. Specifically, for the input molecule m_i , the prompt q_i sequentially includes its SMILES string, its identified FGs, and the predictive rule (see Figure 1 Top-Left). An example of a complete prompt is shown in Figure 3. This prompt enables the LLM to learn the relationship between FGs and the target property. Finally, the LLM is trained on the joint training dataset $\bigcup_{p \in P} D_p^{LLM}$, with $D_p^{LLM} = \{(q_i, y_i)\}_{i=1}^{n_p}$, using

Property	Dataset Size	Dataset Split	
Absorption	Caco-2 Permeability	906	Scaffold
	HIA	578	Scaffold
	Pgp Inhibition	1212	Scaffold
	Bioavailability	640	Scaffold
	Lipophilicity	4200	Scaffold
	Solubility	9982	Scaffold
Distribution	BBB	1975	Scaffold
	PPBR	1797	Scaffold
	VDss	1130	Scaffold
Metabolism	CYP2D6 Inhibition	13130	Scaffold
	CYP3A4 Inhibition	12328	Scaffold
	CYP2C9 Inhibition	12092	Scaffold
	CYP2D6 Substrate	664	Scaffold
	CYP3A4 Substrate	667	Scaffold
	CYP2C9 Substrate	666	Scaffold
Excretion	Half Life	667	Scaffold
	Clearance Microsome	1102	Scaffold
	Clearance Hepatocyte	1020	Scaffold
Toxicity	hERG	648	Scaffold
	Ames Mutagenicity	7255	Scaffold
	DILI	475	Scaffold
	LD50	7385	Scaffold

Table 1: Detailed information and statistics of datasets.

Instruction
A small-molecule drug is a chemical that must travel from the site of administration (e.g., oral) to the site of action (e.g., a tissue), undergo metabolism, and ultimately exit the body. To do this safely and efficaciously, the chemical is required to have numerous ideal absorption, distribution, metabolism, excretion, and toxicity (ADMET) properties. Your task is to predict a specific property of a given drug.

Property Description
Caco-2 Permeability: The human colon epithelial cancer cell line, Caco-2, is used as an in vitro model to simulate the human intestinal tissue. The experimental result on the rate of drug passing through the Caco-2 cells can approximate the rate at which the drug permeates through the human intestinal tissue.

w/ SMILES string
The drug is CNS(=O)(=O)c1ccc(Cl)cc1
Predict its Caco-2 cell effective permeability.

w/ FGs
To support you, you will be provided with all functional groups found in the drug, if any. In this drug, there are 2 Acyl; 2 Amide; 1 Chlorine; 1 Methyl; 1 Sulfonamide; 1 Sulfone

w/ a predictive rule
For your reference, you will be provided with a predictive rule in the form of a tree structure, containing numerous if-then conditions. Hierarchy within the tree is indicated using the number of tab characters (t).
The predictive rule is:
If the number of Hydroxy <= 5.50:
 If the number of Amidine <= 0.50:
 If the number of Acyl Group <= 1.50:
 If the number of Cyclobutane <= 0.50:
 If the number of Hydroxy <= 2.50:
 The Caco-2 Permeability is: -4.70609977117904
 If the number of Hydroxy > 2.50:
 The Caco-2 Permeability is: -5.401695421052631
 If the number of Cyclobutane > 0.50:
 If the number of Homopiperazine <= 0.50:
 The Caco-2 Permeability is: -6.056637875
 If the number of Homopiperazine > 0.50:
 The Caco-2 Permeability is: -6.3000002
 If the number of Acyl Group > 1.50:
 If the number of Ester <= 1.50:
 If the number of Primary Amine <= 0.50:
 The Caco-2 Permeability is: -5.195556619444443
 If the number of Primary Amine > 0.50:
 The Caco-2 Permeability is: -5.617032207692306
 If the number of Ester > 1.50:
 If the number of Carboxamide <= 1.50:
 The Caco-2 Permeability is: -4.423499132
 If the number of Carboxamide > 1.50:
 The Caco-2 Permeability is: -5.332857228571427
 If the number of Amidine > 0.50:
 If the number of Amidrazone <= 1.00:
 If the number of Sulfide <= 0.50:
 If the number of Carboxylic Acid <= 0.50:
 The Caco-2 Permeability is: -6.649803690909092
 If the number of Carboxylic Acid > 0.50:
 The Caco-2 Permeability is: -7.36029675
 If the number of Sulfide > 0.50:
 If the number of Sulfone <= 0.50:
 The Caco-2 Permeability is: -5.930502525
 If the number of Sulfone > 0.50:
 The Caco-2 Permeability is: -6.00942375
 If the number of Amidrazone > 1.00:
 The Caco-2 Permeability is: -4.563333166666667
 If the number of Hydroxy > 5.50:
 If the number of Cyclohexene <= 0.50:
 If the number of Hydroxy <= 10.50:
 If the number of Tetrahydropyran <= 0.50:
 If the number of Enone <= 0.50:
 The Caco-2 Permeability is: -6.8284068
 If the number of Enone > 0.50:
 The Caco-2 Permeability is: -7.13436295
 If the number of Tetrahydropyran > 0.50:
 If the number of Hydroxy <= 7.50:
 The Caco-2 Permeability is: -6.159650883333334
 If the number of Hydroxy > 7.50:
 The Caco-2 Permeability is: -6.617174454545454
 If the number of Hydroxy > 10.50:
 If the number of Ketal <= 0.50:
 The Caco-2 Permeability is: -7.0478787
 If the number of Ketal > 0.50:
 The Caco-2 Permeability is: -7.619999900000002
 If the number of Cyclohexene > 0.50:
 The Caco-2 Permeability is: -4.9000001

Figure 3: An example of a completed prompt used by the proposed method for training LLMs on Caco-2 Permeability. The description of the property is directly adopted from the TDC benchmark’s site¹.

standard next-token cross-entropy loss:

$$L(\theta) = \sum_{p \in P} \sum_{i=1}^{n_p} \sum_{t=1}^{T_i} -\log P_{\theta}(y_i^t | q_i, y_i^{<t}), \quad (1)$$

where θ denotes the LLM parameters, T_i is the total number of tokens in y_i , and y_i^t and $y_i^{<t}$ denote the token at position t and all preceding tokens, respectively. Detailed hyper-parameters for training the LLM are provided in Appendix C.

¹<https://tdcommons.ai>

3.3 Test-Time Scaling

Test-time scaling (Snell et al., 2024) enables an LLM to improve its predictions by allocating extra computation at inference. A notable is self-consistency (Wang et al., 2023), which ensembles N predictions generated from the same prompt via a sampling strategy. Inspired by bagging (Breiman, 1996), we introduce a more sophisticated technique: rule-consistency, which harnesses the diversity among decision trees in a Random Forest (RF) model rather than relying on diversity from the sampling strategy. For each property $p \in P$, we train an RF model consisting of N decision trees and incorporate one randomly selected predictive rule into each prompt while training the LLM (see Figure 1 Bottom-Left). This randomness mirrors the inherent randomness in the RF model, preventing the LLM from depending on individual predictive rules. In inference, for the input molecule m_i , N different predictive rules are used to construct N different prompts, denoted as $\{q_{i,k}\}_{k=1}^N$. Then, rule-consistency ensembles the N predictions generated from these prompts (see Figure 1 Right) to produce the final prediction:

$$\hat{y}_i = \frac{1}{N} \sum_{k=1}^N y_{i,k} \text{ where } y_{i,k} \sim P_{\theta}(y_{i,k}^t | q_{i,k}, y_{i,k}^{<t}). \quad (2)$$

Unless stated otherwise, N is set to 50 to ensure RF models’ robustness and diversity among trees.

Table 2: The results on the TDC benchmark using Gemma-2-2B and Granite-3.3-2B ($N = 50$).

		Metric	Specialist Models		TxGemma-2-2B			Gemma-2-2B	
			MapLight	decision tree	Naive	TreeKD	w/ self-consistency	w/ rule-consistency	
No. trainable parameters		(↓)	-	-	2B	20M	20M	20M	20M
Absorption	Caco-2 Permeability	MAE (↓)	0.269	0.413	0.629	0.547	0.476 (+0.071)	0.551 (-0.075)	0.528 (-0.052)
	HIA	AUROC (↑)	0.982	0.729	0.916	0.820	0.953 (+0.133)	0.956 (+0.003)	0.964 (+0.011)
	Pgp Inhibition	AUROC (↑)	0.931	0.758	0.860	0.818	0.881 (+0.063)	0.886 (+0.005)	0.883 (+0.002)
	Bioavailability	AUROC (↑)	0.751	0.670	0.634	0.692	0.721 (+0.029)	0.725 (+0.004)	0.793 (+0.072)
	Lipophilicity	MAE (↓)	0.547	0.848	0.598	0.672	0.579 (+0.093)	0.634 (-0.055)	0.600 (-0.021)
	Solubility	MAE (↓)	0.793	1.771	0.950	2.921	0.921 (+2.000)	0.982 (-0.061)	0.868 (+0.053)
Distribution	BBB	AUROC (↑)	0.922	0.754	0.869	0.879	0.850 (-0.029)	0.853 (+0.003)	0.906 (+0.056)
	PPBR	MAE (↓)	7.654	11.492	9.986	7.556	7.503 (+0.053)	8.380 (-0.877)	7.459 (+0.044)
	VDss	Spearman (↑)	0.722	0.414	0.387	0.522	0.647 (+0.125)	0.602 (-0.045)	0.675 (+0.028)
Metabolism	CYP2D6 Inhibition	AUPRC (↑)	0.722	0.381	0.590	0.565	0.573 (+0.008)	0.578 (+0.005)	0.591 (+0.018)
	CYP3A4 Inhibition	AUPRC (↑)	0.883	0.629	0.716	0.778	0.841 (+0.063)	0.847 (+0.006)	0.869 (+0.028)
	CYP2C9 Inhibition	AUPRC (↑)	0.785	0.507	0.722	0.696	0.737 (+0.041)	0.741 (+0.004)	0.763 (+0.026)
	CYP2D6 Substrate	AUPRC (↑)	0.713	0.431	0.619	0.569	0.721 (+0.152)	0.604 (-0.117)	0.734 (+0.013)
	CYP3A4 Substrate	AUPRC (↑)	0.702	0.612	0.685	0.668	0.740 (+0.072)	0.730 (-0.010)	0.746 (+0.006)
	CYP2C9 Substrate	AUPRC (↑)	0.422	0.328	0.368	0.553	0.426 (-0.127)	0.431 (+0.005)	0.428 (+0.002)
Excretion	Half Life	Spearman (↑)	0.556	0.007	0.022	0.259	0.272 (+0.013)	0.385 (+0.113)	0.339 (+0.067)
	Clearance Microsome	Spearman (↑)	0.615	0.505	0.504	0.571	0.624 (+0.053)	0.599 (-0.025)	0.611 (-0.013)
	Clearance Hepatocyte	Spearman (↑)	0.459	0.244	0.346	0.421	0.419 (-0.002)	0.360 (-0.059)	0.412 (-0.007)
Toxicity	hERG	AUROC (↑)	0.883	0.600	0.891	0.749	0.848 (+0.099)	0.855 (+0.007)	0.866 (+0.018)
	Ames Mutagenicity	AUROC (↑)	0.864	0.680	0.792	0.766	0.819 (+0.053)	0.823 (+0.004)	0.845 (+0.026)
	DILI	AUROC (↑)	0.892	0.641	0.764	0.717	0.828 (+0.111)	0.831 (+0.003)	0.803 (-0.025)
	LD50	MAE (↓)	0.620	0.805	0.711	0.713	0.680 (+0.033)	0.718 (-0.038)	0.628 (+0.052)

		Metric	Specialist Models		TxGemma-2-2B			Granite-3.3-2B	
			MapLight	decision tree	Naive	TreeKD	w/ self-consistency	w/ rule-consistency	
No. trainable parameters		(↓)	-	-	2B	20M	20M	20M	20M
Absorption	Caco-2 Permeability	MAE (↓)	0.269	0.413	0.629	0.497	0.402 (+0.095)	0.470 (-0.068)	0.432 (-0.030)
	HIA	AUROC (↑)	0.982	0.729	0.916	0.875	0.934 (+0.059)	0.963 (+0.029)	0.957 (+0.023)
	Pgp Inhibition	AUROC (↑)	0.931	0.758	0.860	0.834	0.843 (+0.009)	0.846 (+0.003)	0.900 (+0.057)
	Bioavailability	AUROC (↑)	0.751	0.670	0.634	0.737	0.783 (+0.046)	0.793 (+0.010)	0.788 (+0.005)
	Lipophilicity	MAE (↓)	0.547	0.848	0.598	0.637	0.620 (+0.017)	0.667 (-0.047)	0.597 (+0.023)
	Solubility	MAE (↓)	0.793	1.771	0.950	0.913	0.884 (+0.029)	1.025 (-0.141)	0.855 (+0.029)
Distribution	BBB	AUROC (↑)	0.922	0.754	0.869	0.833	0.870 (+0.037)	0.864 (-0.006)	0.878 (+0.008)
	PPBR	MAE (↓)	7.654	11.492	9.986	8.086	7.259 (+0.827)	8.526 (-1.267)	8.404 (-1.145)
	VDss	Spearman (↑)	0.722	0.414	0.387	0.479	0.574 (+0.095)	0.564 (-0.010)	0.662 (+0.088)
Metabolism	CYP2D6 Inhibition	AUPRC (↑)	0.722	0.381	0.590	0.623	0.600 (-0.023)	0.605 (+0.005)	0.610 (+0.010)
	CYP3A4 Inhibition	AUPRC (↑)	0.883	0.629	0.716	0.810	0.835 (+0.025)	0.842 (+0.007)	0.849 (+0.014)
	CYP2C9 Inhibition	AUPRC (↑)	0.785	0.507	0.722	0.731	0.750 (+0.019)	0.756 (+0.006)	0.772 (+0.022)
	CYP2D6 Substrate	AUPRC (↑)	0.713	0.431	0.619	0.488	0.589 (+0.101)	0.593 (+0.004)	0.609 (+0.020)
	CYP3A4 Substrate	AUPRC (↑)	0.702	0.612	0.685	0.652	0.753 (+0.101)	0.757 (+0.004)	0.719 (-0.034)
	CYP2C9 Substrate	AUPRC (↑)	0.422	0.328	0.368	0.461	0.398 (-0.063)	0.405 (+0.007)	0.487 (+0.089)
Excretion	Half Life	Spearman (↑)	0.556	0.007	0.022	0.293	0.340 (+0.047)	0.324 (-0.016)	0.362 (+0.022)
	Clearance Microsome	Spearman (↑)	0.615	0.505	0.504	0.528	0.663 (+0.135)	0.592 (-0.071)	0.611 (-0.052)
	Clearance Hepatocyte	Spearman (↑)	0.459	0.244	0.346	0.286	0.457 (+0.171)	0.380 (-0.077)	0.483 (+0.026)
Toxicity	hERG	AUROC (↑)	0.883	0.600	0.891	0.720	0.780 (+0.060)	0.793 (+0.013)	0.783 (+0.003)
	Ames Mutagenicity	AUROC (↑)	0.864	0.680	0.792	0.767	0.826 (+0.059)	0.830 (+0.004)	0.831 (+0.005)
	DILI	AUROC (↑)	0.892	0.641	0.764	0.752	0.817 (+0.065)	0.821 (+0.004)	0.798 (-0.019)
	LD50	MAE (↓)	0.620	0.805	0.711	0.686	0.707 (-0.021)	0.753 (-0.046)	0.676 (+0.031)

4 Evaluation

Setup. To evaluate the proposed method, we use two open-source LLMs in the 2B parameters class, i.e., Gemma-2-2B (Team et al., 2024) and Granite-3.3-2B (Granite Team, 2024), and apply LoRA (Hu et al., 2022) to conduct experiments on the

TDC benchmark (Huang et al., 2021) with 22 ADMET properties (listed in Table 1). Each property dataset is split into training, validation, and test sets (see Appendix D for details). We use training sets for fine-tuning LLMs, validation sets for hyper-parameter tuning, and report the results on test sets.

Table 2 presents the results on the TDC benchmark using Gemma-2-2B and Granite-3.3-2B. First, compared to the baseline (using solely the SMILES string in the prompt), TreeKD substantially enhances the performance of LLMs on most properties (19/22 for Gemma-2-2B and 19/22 for Granite-3.3-2B), as indicated in (green). For instance, performance gains on Caco-2 Permeability are +0.071 and +0.095, respectively. Notably, despite the decision tree’s limited performance due to suboptimal configurations (Appendix C), distilling its knowledge into LLMs still yields clear improvements. For instance, while the decision tree achieves only 0.680 on Ames Mutagenicity, TreeKD enables Gemma-2-2B and Granite-3.3-2B to achieve 0.819 and 0.826, respectively, surpassing the baseline scores of 0.766 and 0.767. This finding supports our hypothesis that decision tree knowledge complements the internal knowledge of LLMs, thereby improving their predictive accuracy. Moreover, this suggests that a stronger decision tree could further enhance TreeKD’s effectiveness.

In a head-to-head comparison with TxGemma-2-2B (Wang et al., 2025), the strongest generalist LLM for MPP in the class (built on top of Gemma-2-2B), our method achieves superior performance on most properties (19/22 for Gemma-2-2B and 18/22 for Granite-3.3-2B), as highlighted in bold. Notably, TreeKD significantly narrows the gap with MapLight models² (Notwell and Wood, 2023). For example, on PPBR, the gap decreases from -2.364 (TxGemma-2-2B) to -0.151 and -0.395 for Gemma-2-2B and Granite-3.3-2B, respectively.

The rightmost columns of Table 2 present the results using TreeKD with test-time scaling techniques ($N = 50$). On top of TreeKD, self-consistency only enhances the performance of LLMs further on roughly 50% of properties (12/22 for Gemma-2-2B and 12/22 for Granite-3.3-2B), as indicated in (green) alongside the results. In contrast, rule-consistency further improves performance on most properties (17/22 for Gemma-2-2B and 17/22 for Granite-3.3-2B). This difference stems from self-consistency’s inherent limitation in domain-specific tasks like MPP, where LLMs lack sufficient guidance to ensure meaningful diversity among the N predictions. Overall, rule-consistency clearly outperforms self-consistency on most properties (18/22 for Gemma-2-2B and 17/22 for Granite-3.3-2B), as underlined.

²State-of-the-art specialist models on the TDC benchmark.

Table 3: The performance gains on the TDC benchmark with evolved variants of the prompt.

		Gemma-2-2B		
		Naive	Naive w/ FGs	Naive w/ FGs w/ a predictive rule (TreeKD)
Absorption	Caco-2 Permeability	0.547	+0.055	+0.016
	HIA	0.820	+0.065	+0.068
	Pgp Inhibition	0.818	+0.049	+0.014
	Bioavailability	0.692	+0.059	-0.030
	Lipophilicity	0.672	-0.005	+0.098
	Solubility	2.921	+2.012	-0.012
Distribution	BBB	0.879	-0.026	-0.003
	PPBR	7.556	-1.657	+1.710
	VDss	0.522	+0.043	+0.082
Metabolism	CYP2D6 Inhibition	0.565	+0.028	-0.020
	CYP3A4 Inhibition	0.778	+0.040	+0.023
	CYP2C9 Inhibition	0.696	+0.023	+0.018
	CYP2D6 Substrate	0.569	+0.023	+0.129
	CYP3A4 Substrate	0.668	+0.046	+0.026
	CYP2C9 Substrate	0.553	-0.109	-0.018
Excretion	Half Life	0.259	+0.158	-0.145
	Clearance Microsome	0.571	+0.026	+0.027
	Clearance Hepatocyte	0.421	-0.135	+0.133
Toxicity	hERG	0.749	+0.041	+0.058
	Ames Mutagenicity	0.766	+0.029	+0.024
	DILI	0.717	+0.051	+0.060
	LD50	0.713	-0.007	+0.040

		Granite-3.3-2B		
		Naive	Naive w/ FGs	Naive w/ FGs w/ a predictive rule (TreeKD)
Absorption	Caco-2 Permeability	0.497	+0.072	+0.023
	HIA	0.875	+0.064	-0.005
	Pgp Inhibition	0.834	+0.012	-0.003
	Bioavailability	0.737	+0.005	+0.041
	Lipophilicity	0.637	+0.004	+0.013
	Solubility	0.913	+0.006	+0.023
Distribution	BBB	0.833	-0.024	+0.061
	PPBR	8.086	-1.024	+1.851
	VDss	0.479	+0.059	+0.036
Metabolism	CYP2D6 Inhibition	0.623	-0.025	+0.002
	CYP3A4 Inhibition	0.810	+0.007	+0.018
	CYP2C9 Inhibition	0.731	+0.016	+0.003
	CYP2D6 Substrate	0.488	+0.068	+0.033
	CYP3A4 Substrate	0.652	+0.002	+0.099
	CYP2C9 Substrate	0.461	-0.093	+0.030
Excretion	Half Life	0.293	-0.020	+0.067
	Clearance Microsome	0.528	+0.078	+0.057
	Clearance Hepatocyte	0.286	+0.017	+0.154
Toxicity	hERG	0.720	+0.091	-0.031
	Ames Mutagenicity	0.767	+0.037	+0.022
	DILI	0.752	+0.033	+0.032
	LD50	0.686	-0.029	+0.008

5 Ablation Study

Setup. In TreeKD, the prompt that is associated with an input molecule sequentially includes its SMILES string, its found FGs, and a predictive

	No. samples predicted accurately	No. samples predicted inaccurately
decision tree	902	555
Gemma-2-2B TreeKD	722	180
Granite-3.3-2B TreeKD	748	154

Figure 4: The arrangements of 1457 molecules in the testing set according to whether a molecule is predicted accurately.

rule, as exemplified in Figure 3. Therefore, to better understand the effect of the proposed method, we conduct ablatinal experiments on the TDC benchmark using evolved variants of the prompt and sequentially measure performance gains. Note that using solely the SMILES string in the prompt simply reflects the naive method.

Table 3 presents the performance gains on the TDC benchmark using Gemma-2-2B and Granite-3.3-2B. Noticeably, providing LLMs with all FGs found in the molecule enhances their performance on most properties (16/22 for Gemma-2-2B and 16/22 for Granite-3.3-2B). This is likely due to the activation of their understanding of the relationship between found FGs and the properties (Wellawatte and Schwaller, 2025), which is acquired in the pre-training phase. On top of that, providing LLMs with the predictive rule (TreeKD) also enhances the performance of LLMs on most properties (16/22 for Gemma-2-2B and 19/22 for Granite-3.3-2B). For instance, performance gains of TreeKD over the naive method on Caco-2 Permeability derived in the previous section, i.e., +0.071 and +0.095, of which +0.055 and +0.072, respectively, are attributable to providing LLMs with all FGs found in the molecule.

6 Analysis of Rule Utilization

Although decision tree knowledge complements the internal knowledge of LLMs, this knowledge also has limitations (as the decision tree’s performance is bounded) and can therefore be misleading. Thus, LLMs must use the predictive rule in a wise manner, especially when it fails. To examine this, we analyze Ames Mutagenicity (a toxicity property), where the decision tree achieves only 0.680, yet TreeKD enables Gemma-2-2B and Granite-3.3-2B to achieve 0.819 and 0.826, respectively, as reported earlier. Figure 4 illustrates the distribution of 1457 molecules in the test set according to whether each molecule is predicted correctly.

	No. samples predicted accurately	No. samples predicted inaccurately
Gemma-2-2B Naive	13	17
Gemma-2-2B TreeKD	20	10
Granite-3.3-2B Naive	13	17
Granite-3.3-2B TreeKD	18	12

Figure 5: The arrangements of 30 pairs of molecules exhibiting property cliffs in the testing set according to whether both molecules in each pair are predicted accurately.

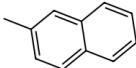
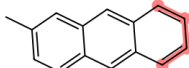
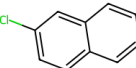
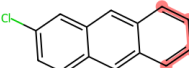
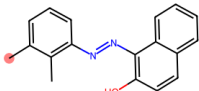
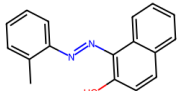
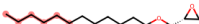
		
	Ames Mutagenicity: No	Ames Mutagenicity: Yes
Gemma-2-2B Naive	No ✓	No ✗
Gemma-2-2B TreeKD	No ✓	Yes ✓
Granite-3.3-2B Naive	No ✓	No ✗
Granite-3.3-2B TreeKD	No ✓	Yes ✓
		
	Ames Mutagenicity: No	Ames Mutagenicity: Yes
Gemma-2-2B Naive	No ✓	No ✗
Gemma-2-2B TreeKD	No ✓	Yes ✓
Granite-3.3-2B Naive	No ✓	No ✗
Granite-3.3-2B TreeKD	No ✓	Yes ✓
		
	Ames Mutagenicity: No	Ames Mutagenicity: Yes
Gemma-2-2B Naive	Yes ✗	Yes ✓
Gemma-2-2B TreeKD	No ✓	Yes ✓
Granite-3.3-2B Naive	Yes ✗	Yes ✓
Granite-3.3-2B TreeKD	No ✓	Yes ✓
		
	Ames Mutagenicity: No	Ames Mutagenicity: Yes
Gemma-2-2B Naive	Yes ✗	Yes ✓
Gemma-2-2B TreeKD	No ✓	Yes ✓
Granite-3.3-2B Naive	Yes ✗	Yes ✓
Granite-3.3-2B TreeKD	No ✓	Yes ✓

Figure 6: A few examples of pairs of molecules exhibiting property cliffs in the testing set (differences are highlighted in red), showing whether both molecules in each pair are predicted accurately.

Among the 555 molecules incorrectly predicted by the decision tree, TreeKD still enables Gemma-2-2B and Granite-3.3-2B to correctly predict the majority (371/555 and 357/555, respectively). This demonstrates that LLMs do not blindly follow the predictive rule but instead use it wisely, especially when it fails.

Furthermore, we assume that TreeKD improves LLMs’ ability to capture the concept of property cliffs. To examine this hypothesis, we conduct an additional analysis on Ames Mutagenicity. First, we identify pairs of molecules exhibiting property cliffs in the test set, where each pair consists of two

Table 4: The results on the TDC benchmark using TreeKD with test-time scaling techniques ($N = 50$ and $N = 100$). Note that * stands for consistency.

		Gemma-2-2B			
		$N = 50$		$N = 100$	
		self-*	rule-*	self-*	rule-*
Absorption	Caco-2 Permeability	0.551	<u>0.528</u>	0.537 (+0.014)	0.520 (+0.008)
	HIA	0.956	<u>0.964</u>	0.959 (+0.003)	0.965 (+0.001)
	Pgp Inhibition	<u>0.886</u>	0.883	0.880 (-0.006)	0.879 (-0.004)
	Bioavailability	0.725	<u>0.793</u>	0.729 (+0.004)	0.792 (-0.001)
	Lipophilicity	0.634	<u>0.600</u>	0.627 (+0.007)	0.595 (+0.005)
	Solubility	0.982	<u>0.868</u>	0.978 (+0.004)	0.869 (-0.001)
	Distribution	BBB	0.853	<u>0.906</u>	0.850 (-0.003)
	PPBR	8.380	<u>7.459</u>	7.913 (+0.467)	7.329 (+0.130)
	VDss	0.602	<u>0.675</u>	0.594 (-0.008)	0.670 (-0.005)
Metabolism	CYP2D6 Inhibition	0.578	<u>0.591</u>	0.575 (-0.003)	0.593 (+0.002)
	CYP3A4 Inhibition	0.847	<u>0.869</u>	0.841 (-0.006)	0.868 (-0.001)
	CYP2C9 Inhibition	0.741	<u>0.763</u>	0.748 (+0.007)	0.767 (+0.004)
	CYP2D6 Substrate	0.604	<u>0.734</u>	0.602 (-0.002)	0.736 (+0.002)
	CYP3A4 Substrate	0.730	<u>0.746</u>	0.731 (+0.001)	0.748 (+0.002)
	CYP2C9 Substrate	<u>0.431</u>	0.428	<u>0.432</u> (+0.001)	0.429 (+0.001)
	Excretion	Half Life	<u>0.385</u>	0.339	<u>0.412</u> (+0.027)
	Clearance Microsome	0.599	<u>0.611</u>	<u>0.609</u> (+0.010)	0.600 (-0.011)
	Clearance Hepatocyte	0.360	<u>0.412</u>	0.339 (-0.021)	<u>0.402</u> (-0.010)
Toxicity	hERG	0.855	<u>0.866</u>	0.854 (-0.001)	0.870 (+0.004)
	Ames Mutagenicity	0.823	<u>0.845</u>	0.820 (-0.003)	0.845 (+0.000)
	DILI	<u>0.831</u>	0.803	0.830 (-0.001)	0.800 (-0.003)
	LD50	0.718	<u>0.628</u>	0.719 (-0.001)	0.627 (+0.001)
		Granite-3.3-2B			
		$N = 50$		$N = 100$	
		self-*	rule-*	self-*	rule-*
Absorption	Caco-2 Permeability	0.470	<u>0.432</u>	0.461 (+0.009)	0.426 (+0.006)
	HIA	<u>0.963</u>	0.957	<u>0.969</u> (+0.006)	0.959 (+0.002)
	Pgp Inhibition	0.846	<u>0.900</u>	0.842 (-0.004)	0.903 (+0.003)
	Bioavailability	<u>0.793</u>	0.788	0.791 (-0.002)	0.782 (-0.006)
	Lipophilicity	0.667	<u>0.597</u>	0.666 (+0.001)	0.596 (+0.001)
	Solubility	1.025	<u>0.855</u>	0.980 (+0.045)	<u>0.857</u> (-0.002)
	Distribution	BBB	0.864	<u>0.878</u>	0.861 (-0.003)
	PPBR	8.526	<u>8.404</u>	7.991 (+0.535)	8.208 (+0.196)
	VDss	0.564	<u>0.662</u>	0.569 (+0.005)	0.655 (-0.007)
Metabolism	CYP2D6 Inhibition	0.605	<u>0.610</u>	0.600 (-0.005)	0.611 (+0.001)
	CYP3A4 Inhibition	0.842	<u>0.849</u>	0.844 (+0.002)	0.847 (-0.002)
	CYP2C9 Inhibition	0.756	<u>0.772</u>	0.760 (+0.004)	0.776 (+0.004)
	CYP2D6 Substrate	0.593	<u>0.609</u>	0.591 (-0.002)	0.609 (+0.000)
	CYP3A4 Substrate	<u>0.757</u>	0.719	0.760 (+0.003)	0.720 (+0.001)
	CYP2C9 Substrate	0.405	<u>0.487</u>	0.461 (+0.056)	0.489 (+0.002)
	Excretion	Half Life	0.324	<u>0.362</u>	0.300 (-0.024)
	Clearance Microsome	0.592	<u>0.611</u>	0.572 (-0.020)	0.618 (+0.007)
	Clearance Hepatocyte	0.380	<u>0.483</u>	0.407 (+0.027)	<u>0.477</u> (-0.006)
Toxicity	hERG	<u>0.793</u>	0.783	0.792 (-0.001)	0.777 (-0.006)
	Ames Mutagenicity	0.830	<u>0.831</u>	0.828 (-0.002)	0.830 (-0.001)
	DILI	<u>0.821</u>	0.798	0.820 (-0.001)	0.796 (-0.002)
	LD50	0.753	<u>0.676</u>	0.755 (-0.002)	0.670 (+0.006)

molecules with a Tanimoto similarity (Bajusz et al., 2015) greater than 0.8 but with opposite properties. Figure 5 illustrates the distribution of 30 such pairs according to whether both molecules in each pair are predicted correctly. Among these 30 pairs,

TreeKD enables Gemma-2-2B and Granite-3.3-2B to correctly predict both molecules in considerably more pairs (20/30 and 18/30, respectively) than the baseline (13/30 for both). This suggests that TreeKD improves LLMs’ ability to capture the concept of property cliffs (see Figure 6 for examples).

7 Test-Time Scaling Analysis

In the previous section, we investigated the impact of test-time scaling techniques on TreeKD with $N = 50$. Here, we discuss their scaling behavior with $N = 100$. Table 4 presents the results on the TDC benchmark using TreeKD with test-time scaling techniques ($N = 50$ and $N = 100$). Compared to $N = 50$, self-consistency exhibits modest scaling behavior, further improving LLM performance on only 50% of properties (11/22 for Gemma-2-2B and 11/22 for Granite-3.3-2B), as indicated in (green). Similarly, rule-consistency exhibits modest scaling behavior, further improving performance on approximately 50% of properties (12/22 for Gemma-2-2B and 13/22 for Granite-3.3-2B). Upon closer examination, LLM performance tends to converge with marginal variations. This may be explained by similar behavior in RF models, whose performance also converges with $N = 100$ (Appendix B). Specifically, the diversity among decision trees in RF models may saturate. Nevertheless, with $N = 100$, rule-consistency clearly outperforms self-consistency on most properties (17/22 for Gemma-2-2B and 16/22 for Granite-3.3-2B), as underlined.

8 Conclusion

We presented TreeKD, a knowledge distillation method that transfers complementary knowledge from tree-based specialist models to LLMs by verbalizing decision tree rules as natural language. We further introduced rule-consistency, a test-time scaling technique that ensembles predictions across diverse rules from a Random Forest. Experiments on 22 ADMET properties demonstrate that TreeKD substantially improves LLM performance, outperforming TxGemma-2-2B and narrowing the gap with state-of-the-art specialist models. Importantly, our findings suggest that combining traditional machine learning models and LLMs offers a promising direction for advancing generalist models for molecular property prediction.

Limitations

One limitation of our proposed method is the increased training cost due to lengthy prompts caused by the predictive rule. Nonetheless, by applying an efficient training recipe with advanced techniques like vLLM (Kwon et al., 2023), this cost remains manageable, allowing all experiments to be conducted on 2 NVIDIA A100 80GB GPUs. In inference, since the predictive rule is static at the prefix, caching techniques (Gim et al., 2024; Zheng et al., 2024) can be applied to reduce inference cost. Also, expanding the scope to include tens or hundreds of properties, as well as generalizing the proposed approach to other tasks within the drug discovery pipeline and to additional entities such as proteins or nucleic acids (Ferreira and Carneiro, 2025), constitutes an important direction for future work.

References

- Josh Achiam, Steven Adler, Sandhini Agarwal, Lama Ahmad, Ilge Akkaya, Florencia Leoni Aleman, Diogo Almeida, Janko Altenschmidt, Sam Altman, Shyamal Anadkat, and 1 others. 2023. Gpt-4 technical report. *arXiv preprint arXiv:2303.08774*.
- PR Andrews, DJ Craik, and JL Martin. 1984. Functional group contributions to drug-receptor interactions. *Journal of medicinal chemistry*, 27(12):1648–1657.
- Dávid Bajusz, Anita Rácz, and Károly Héberger. 2015. Why is tanimoto index an appropriate choice for fingerprint-based similarity calculations? *Journal of cheminformatics*, 7(1):20.
- Leo Breiman. 1996. Bagging predictors. *Machine learning*, 24(2):123–140.
- Tom Brown, Benjamin Mann, Nick Ryder, Melanie Subbiah, Jared D Kaplan, Prafulla Dhariwal, Arvind Neelakantan, Pranav Shyam, Girish Sastry, Amanda Askell, and 1 others. 2020. Language models are few-shot learners. *Advances in neural information processing systems*, 33:1877–1901.
- He Cao, Zijing Liu, Xingyu Lu, Yuan Yao, and Yu Li. 2025. InstructMol: Multi-modal integration for building a versatile and reliable molecular assistant in drug discovery. In *Proceedings of the 31st International Conference on Computational Linguistics*, pages 354–379, Abu Dhabi, UAE. Association for Computational Linguistics.
- Cayque Monteiro Castro Nascimento and André Silva Pimentel. 2023. Do large language models understand chemistry? a conversation with chatgpt. *Journal of Chemical Information and Modeling*, 63(6):1649–1655.
- Sahil Chaudhary. 2023. Code alpaca: An instruction-following llama model for code generation. <https://github.com/sahil280114/codealpaca>.
- Juan Manuel Zambrano Chaves, Eric Wang, Tao Tu, Eeshit Dhaval Vaishnav, Byron Lee, S Sara Mahdavi, Christopher Sementurs, David Fleet, Vivek Nataraajan, and Shekoofeh Azizi. 2024. Tx-llm: A large language model for therapeutics. *arXiv preprint arXiv:2406.06316*.
- Wei-Lin Chiang, Zhuohan Li, Zi Lin, Ying Sheng, Zhanghao Wu, Hao Zhang, Lianmin Zheng, Siyuan Zhuang, Yonghao Zhuang, Joseph E. Gonzalez, Ion Stoica, and Eric P. Xing. 2023. Vicuna: An open-source chatbot impressing gpt-4 with 90%* chatgpt quality.
- Gheorghe Comanici, Eric Bieber, Mike Schaeckermann, Ice Pasupat, Noveen Sachdeva, Inderjit Dhillon, Marcel Blistein, Ori Ram, Dan Zhang, Evan Rosen, and 1 others. 2025. Gemini 2.5: Pushing the frontier with advanced reasoning, multimodality, long context, and next generation agentic capabilities. *arXiv preprint arXiv:2507.06261*.
- Yin Fang, Xiaozhuan Liang, Ningyu Zhang, Kangwei Liu, Rui Huang, Zhuo Chen, Xiaohui Fan, and Hua-jun Chen. 2024. Mol-instructions: A large-scale biomolecular instruction dataset for large language models. In *The Twelfth International Conference on Learning Representations*.
- Fábio JN Ferreira and Agnaldo S Carneiro. 2025. AI-driven drug discovery: A comprehensive review. *ACS omega*.
- Leonardo LG Ferreira and Adriano D Andricopulo. 2019. Admet modeling approaches in drug discovery. *Drug discovery today*, 24(5):1157–1165.
- In Gim, Guojun Chen, Seung-seob Lee, Nikhil Sarda, Anurag Khandelwal, and Lin Zhong. 2024. Prompt cache: Modular attention reuse for low-latency inference. *Proceedings of Machine Learning and Systems*, 6:325–338.
- IBM Granite Team. 2024. Granite 3.0 language models. <https://github.com/ibm-granite/granite-3.0-language-models>.
- Yuxian Gu, Li Dong, Furu Wei, and Minlie Huang. 2024. MiniLLM: Knowledge distillation of large language models. In *The Twelfth International Conference on Learning Representations*.
- Taicheng Guo, Bozhao Nan, Zhenwen Liang, Zhichun Guo, Nitesh Chawla, Olaf Wiest, Xiangliang Zhang, and 1 others. 2023. What can large language models do in chemistry? a comprehensive benchmark on eight tasks. *Advances in Neural Information Processing Systems*, 36:59662–59688.
- Torben Gutermuth, Patrick Penner, Jochen Sieg, Uschi Dolfus, and Matthias Rarey. 2025. Smartchemist-simplifying communication about organic chemical

- structures. *Journal of Chemical Information and Modeling*.
- Dan Hendrycks, Collin Burns, Steven Basart, Andy Zou, Mantas Mazeika, Dawn Song, and Jacob Steinhardt. 2021. Measuring massive multitask language understanding. In *International Conference on Learning Representations*.
- Geoffrey Hinton, Oriol Vinyals, and Jeff Dean. 2015. Distilling the knowledge in a neural network. *arXiv preprint arXiv:1503.02531*.
- Edward J Hu, Yelong Shen, Phillip Wallis, Zeyuan Allen-Zhu, Yuanzhi Li, Shean Wang, Lu Wang, Weizhu Chen, and 1 others. 2022. Lora: Low-rank adaptation of large language models. *ICLR*, 1(2):3.
- Kexin Huang, Tianfan Fu, Wenhao Gao, Yue Zhao, Yusuf Roohani, Jure Leskovec, Connor W Coley, Cao Xiao, Jimeng Sun, and Marinka Zitnik. 2021. Therapeutics data commons: Machine learning datasets and tasks for drug discovery and development. *arXiv preprint arXiv:2102.09548*.
- Yoon Kim and Alexander M Rush. 2016. Sequence-level knowledge distillation. In *Proceedings of the 2016 conference on empirical methods in natural language processing*, pages 1317–1327.
- Diederik P. Kingma and Jimmy Ba. 2017. [Adam: A method for stochastic optimization](#). *Preprint*, arXiv:1412.6980.
- Woosuk Kwon, Zhuohan Li, Siyuan Zhuang, Ying Sheng, Lianmin Zheng, Cody Hao Yu, Joseph E. Gonzalez, Hao Zhang, and Ion Stoica. 2023. Efficient memory management for large language model serving with pagedattention. In *Proceedings of the ACM SIGOPS 29th Symposium on Operating Systems Principles*.
- Khiem Le, Zhichun Guo, Kaiwen Dong, Xiaobao Huang, Bozhao Nan, Roshni Iyer, Xiangliang Zhang, Olaf Wiest, Wei Wang, and Nitesh V Chawla. 2024. Molx: Enhancing large language models for molecular learning with a multi-modal extension. *arXiv preprint arXiv:2406.06777*.
- Junnan Li, Dongxu Li, Silvio Savarese, and Steven Hoi. 2023. Blip-2: Bootstrapping language-image pre-training with frozen image encoders and large language models. In *International conference on machine learning*, pages 19730–19742. PMLR.
- Sihang Li, Zhiyuan Liu, Yanchen Luo, Xiang Wang, Xiangnan He, Kenji Kawaguchi, Tat-Seng Chua, and Qi Tian. 2024. Towards 3d molecule-text interpretation in language models. In *The Twelfth International Conference on Learning Representations*.
- Yuyan Liu, Sirui Ding, Sheng Zhou, Wenqi Fan, and Qiaoyu Tan. 2024. Moleculargpt: Open large language model (llm) for few-shot molecular property prediction. *arXiv preprint arXiv:2406.12950*.
- Zhiyuan Liu, Sihang Li, Yanchen Luo, Hao Fei, Yixin Cao, Kenji Kawaguchi, Xiang Wang, and Tat-Seng Chua. 2023. MolCA: Molecular graph-language modeling with cross-modal projector and uni-modal adapter. In *Proceedings of the 2023 Conference on Empirical Methods in Natural Language Processing*, pages 15623–15638, Singapore. Association for Computational Linguistics.
- Tanya Liyaqat, Tanvir Ahmad, and Chandni Saxena. 2025. Advancements in molecular property prediction: A survey of single and multimodal approaches: T. liyaqat et al. *Archives of Computational Methods in Engineering*, pages 1–31.
- Gerald M Maggiora. 2006. On outliers and activity cliffs why qsar often disappoints.
- Sewon Min, Mike Lewis, Luke Zettlemoyer, and Han-naneh Hajishirzi. 2022. MetaICL: Learning to learn in context. In *Proceedings of the 2022 Conference of the North American Chapter of the Association for Computational Linguistics: Human Language Technologies*, pages 2791–2809, Seattle, United States. Association for Computational Linguistics.
- James H Notwell and Michael W Wood. 2023. Admet property prediction through combinations of molecular fingerprints. *arXiv preprint arXiv:2310.00174*.
- Fabian Pedregosa, Gaël Varoquaux, Alexandre Gramfort, Vincent Michel, Bertrand Thirion, Olivier Grisel, Mathieu Blondel, Peter Prettenhofer, Ron Weiss, Vincent Dubourg, and 1 others. 2011. Scikit-learn: Machine learning in python. *the Journal of machine Learning research*, 12:2825–2830.
- Nicholas T Runcie, Charlotte M Deane, and Fer-gus Imrie. 2025. Assessing the chemical intelligence of large language models. *arXiv preprint arXiv:2505.07735*.
- Robert Schmidt, Emanuel SR Ehmki, Farina Ohm, Hans-Christian Ehrlich, Andriy Mashychev, and Matthias Rarey. 2019. Comparing molecular patterns using the example of smarts: theory and algorithms. *Journal of Chemical Information and Modeling*, 59(6):2560–2571.
- Charlie Snell, Jaehoon Lee, Kelvin Xu, and Aviral Kumar. 2024. Scaling llm test-time compute optimally can be more effective than scaling model parameters. *arXiv preprint arXiv:2408.03314*.
- Dagmar Stumpfe and Jurgen Bajorath. 2012. Exploring activity cliffs in medicinal chemistry: miniperspective. *Journal of medicinal chemistry*, 55(7):2932–2942.
- Mirac Suzgun, Nathan Scales, Nathanael Schärli, Sebastian Gehrmann, Yi Tay, Hyung Won Chung, Aakanksha Chowdhery, Quoc Le, Ed Chi, Denny Zhou, and Jason Wei. 2023. Challenging BIG-bench tasks and whether chain-of-thought can solve them. In *Findings of the Association for Computational Linguistics: ACL 2023*, pages 13003–13051, Toronto, Canada. Association for Computational Linguistics.

- Rohan Taori, Ishaan Gulrajani, Tianyi Zhang, Yann Dubois, Xuechen Li, Carlos Guestrin, Percy Liang, and Tatsunori B. Hashimoto. 2023. Stanford alpaca: An instruction-following llama model. https://github.com/tatsu-lab/stanford_alpaca.
- Gemma Team, Morgane Riviere, Shreya Pathak, Pier Giuseppe Sessa, Cassidy Hardin, Surya Bhupatiraju, Léonard Hussenot, Thomas Mesnard, Bobak Shahriari, Alexandre Ramé, and 1 others. 2024. Gemma 2: Improving open language models at a practical size. *arXiv preprint arXiv:2408.00118*.
- Eric Wang, Samuel Schmidgall, Paul F Jaeger, Fan Zhang, Rory Pilgrim, Yossi Matias, Joelle Barral, David Fleet, and Shekoofeh Azizi. 2025. Txxgemma: Efficient and agentic llms for therapeutics. *arXiv preprint arXiv:2504.06196*.
- Xuezhi Wang, Jason Wei, Dale Schuurmans, Quoc V Le, Ed H. Chi, Sharan Narang, Aakanksha Chowdhery, and Denny Zhou. 2023. Self-consistency improves chain of thought reasoning in language models. In *The Eleventh International Conference on Learning Representations*.
- Geemi P Wellawatte and Philippe Schwaller. 2025. Human interpretable structure-property relationships in chemistry using explainable machine learning and large language models. *Communications Chemistry*, 8(1):11.
- Zhenqin Wu, Bharath Ramsundar, Evan N Feinberg, Joseph Gomes, Caleb Geniesse, Aneesh S Pappu, Karl Leswing, and Vijay Pande. 2018. Moleculenet: a benchmark for molecular machine learning. *Chemical science*, 9(2):513–530.
- Jun Xia, Lecheng Zhang, Xiao Zhu, Yue Liu, Zhangyang Gao, Bozhen Hu, Cheng Tan, Jiangbin Zheng, Siyuan Li, and Stan Z Li. 2023. Understanding the limitations of deep models for molecular property prediction: Insights and solutions. *Advances in Neural Information Processing Systems*, 36:64774–64792.
- Yingce Xia, Peiran Jin, Shufang Xie, Liang He, Chuan Cao, Renqian Luo, Guoqing Liu, Yue Wang, Zequn Liu, Yuan-Jyue Chen, and 1 others. 2025. Nature language model: Deciphering the language of nature for scientific discovery. *arXiv preprint arXiv:2502.07527*.
- Wei Yao, Wenkai Yang, Ziqiao Wang, Yankai Lin, and Yong Liu. 2025. Revisiting weak-to-strong generalization in theory and practice: Reverse KL vs. forward KL. In *Findings of the Association for Computational Linguistics: ACL 2025*, pages 2860–2888, Vienna, Austria. Association for Computational Linguistics.
- Botao Yu, Frazier N. Baker, Ziqi Chen, Xia Ning, and Huan Sun. 2024. LlaSMol: Advancing large language models for chemistry with a large-scale, comprehensive, high-quality instruction tuning dataset. In *First Conference on Language Modeling*.
- Qiang Zhang, Keyan Ding, Tianwen Lv, Xinda Wang, Qingyu Yin, Yiwen Zhang, Jing Yu, Yuhao Wang, Xiaotong Li, Zhuoyi Xiang, and 1 others. 2025. Scientific large language models: A survey on biological & chemical domains. *ACM Computing Surveys*, 57(6):1–38.
- Lianmin Zheng, Liangsheng Yin, Zhiqiang Xie, Chuyue Livia Sun, Jeff Huang, Cody Hao Yu, Shiyi Cao, Christos Kozyrakis, Ion Stoica, Joseph E Gonzalez, and 1 others. 2024. Sglang: Efficient execution of structured language model programs. *Advances in neural information processing systems*, 37:62557–62583.
- Zhiqiang Zhong, Kuangyu Zhou, and Davide Motin. 2024. Benchmarking large language models for molecule prediction tasks. *arXiv preprint arXiv:2403.05075*.

Table 5: The results on the TDC benchmark using RF models ($N = 50$ and $N = 100$).

		RF	
		$N = 50$	$N = 100$
Absorption	Caco-2 Permeability	0.355	0.354 (+0.001)
	HIA	0.853	0.849 (-0.004)
	Pgp Inhibition	0.845	0.874 (+0.029)
	Bioavailability	0.723	0.621 (-0.101)
	Lipophilicity	0.842	0.841 (+0.001)
	Solubility	1.702	1.703 (-0.001)
Distribution	BBB	0.848	0.839 (-0.009)
	PPBR	11.043	11.123 (-0.080)
	VDss	0.489	0.491 (+0.002)
Metabolism	CYP2D6 Inhibition	0.360	0.395 (+0.035)
	CYP3A4 Inhibition	0.642	0.657 (+0.014)
	CYP2C9 Inhibition	0.481	0.542 (+0.061)
	CYP2D6 Substrate	0.559	0.559 (+0.000)
	CYP3A4 Substrate	0.628	0.654 (+0.026)
	CYP2C9 Substrate	0.323	0.371 (+0.048)
Excretion	Half Life	0.259	0.257 (-0.001)
	Clearance Microsome	0.539	0.544 (+0.005)
	Clearance Hepatocyte	0.363	0.351 (-0.011)
Toxicity	hERG	0.698	0.694 (-0.003)
	Ames Mutagenicity	0.732	0.757 (+0.026)
	DILI	0.719	0.679 (-0.040)
	LD50	0.776	0.774 (+0.002)

A Hyper-parameters of Specialist Models

For each property $p \in P$, the decision tree r_p as well as decision trees in the RF model are trained on the training dataset $D_p^{FGS} = \{(v_i, y_i)\}_{i=1}^{n_p}$. Each decision tree has a maximum depth of 6 (`max_depth = 6`). Also, the minimum number of samples required to split an internal node is set to 2 (`min_samples_split = 2`), and the minimum number of samples required to be at a leaf node is set to 1 (`min_samples_leaf = 1`). All other hyper-parameters are set to their default values as implemented in scikit-learn (Pedregosa et al., 2011).

B RF Models

Table 5 presents the results on the TDC benchmark using RF models, with $N = 50$ and $N = 100$. It should be noted that, with $N = 100$, RF models have better performance on roughly 50% of properties (13/22), as indicated in (green) alongside the results. Also, their performance tends to converge with marginal variations.

C Training Details of LLMs

As mentioned above, both Gemma-2-2B and Granite-3.3-2B are trained on the joint training dataset using Low-Rank Adaptation (LoRA) (Hu et al., 2022). LoRA adapter is applied to all Lin-

ear modules except the generation head, with the `lora_rank` is set to 16 and `lora_alpha` is set to 32. The LLMs are trained in 8 epochs by the Adam optimizer (Kingma and Ba, 2017) (`weight_decay` is 0) with the `learning_rate` of $1e-5$, which is linearly reduced to $1e-6$ throughout the training process. Notably, prompts are truncated to a maximum length of 1024 tokens. A single run of training with a batch size of 8 is carried out on 2 NVIDIA A100 80GB GPUs in 20 hours.

D Datasets

TDC benchmark (Therapeutics Data Commons) (Huang et al., 2021) is a resource for accessing standardized datasets to evaluate AI methods, supporting the identification of which methods are most suitable for Drug Discovery and why. Concentrating on MPP, we utilize 22 datasets corresponding to 22 ADMET properties, particularly including Caco-2 Permeability, HIA (Human Intestinal Absorption), Pgp (P-glycoprotein) Inhibition, Bioavailability, Lipophilicity, Solubility, BBB (Blood-Brain Barrier), PPBR (Plasma Protein Binding Rate), VDss (Volume of Distribution at steady state), CYP2D6 Inhibition, CYP3A4 Inhibition, CYP2C9 Inhibition, CYP2D6 Substrate, CYP3A4 Substrate, CYP2C9 Substrate, Half Life, Clearance Microsome, Clearance Hepatocyte, hERG (Human Ether-a-go-go-related Gene), Ames Mutagenicity, DILI (Drug Induced Liver Injury), LD50 (Lethal Dose 50%). The descriptions of these properties are shown in Table 6.

Table 6: Detailed descriptions of the properties.

Property	Property Description	
Absorption	Caco-2 Permeability	The human colon epithelial cancer cell line, Caco-2, is used as an in vitro model to simulate the human intestinal tissue. The experimental result on the rate of drug passing through the Caco-2 cells can approximate the rate at which the drug permeates through the human intestinal tissue.
	HIA	When a drug is orally administered, it needs to be absorbed from the human gastrointestinal system into the bloodstream of the human body. This ability of absorption is called human intestinal absorption (HIA) and it is crucial for a drug to be delivered to the target.
	Pgp Inhibition	P-glycoprotein (Pgp) is an ABC transporter protein involved in intestinal absorption, drug metabolism, and brain penetration, and its inhibition can seriously alter a drug's bioavailability and safety. In addition, inhibitors of Pgp can be used to overcome multidrug resistance.
	Bioavailability	Oral bioavailability is defined as "the rate and extent to which the active ingredient or active moiety is absorbed from a drug product and becomes available at the site of action".
	Lipophilicity	Lipophilicity measures the ability of a drug to dissolve in a lipid (e.g. fats, oils) environment. High lipophilicity often leads to high rate of metabolism, poor solubility, high turn-over, and low absorption.
	Solubility	Aqueous solubility measures a drug's ability to dissolve in water. Poor water solubility could lead to slow drug absorptions, inadequate bioavailability and even induce toxicity. More than 40% of new chemical entities are not soluble.
Distribution	BBB	As a membrane separating circulating blood and brain extracellular fluid, the blood-brain barrier (BBB) is the protection layer that blocks most foreign drugs. Thus the ability of a drug to penetrate the barrier to deliver to the site of action forms a crucial challenge in development of drugs for central nervous system.
	PPBR	The human plasma protein binding rate (PPBR) is expressed as the percentage of a drug bound to plasma proteins in the blood. This rate strongly affect a drug's efficiency of delivery. The less bound a drug is, the more efficiently it can traverse and diffuse to the site of actions.
	VDss	The volume of distribution at steady state (VDss) measures the degree of a drug's concentration in body tissue compared to concentration in blood. Higher VD indicates a higher distribution in the tissue and usually indicates the drug with high lipid solubility, low plasma protein binding rate.
Metabolism	CYP2D6 Inhibition	The CYP P450 genes are involved in the formation and breakdown (metabolism) of various molecules and chemicals within cells. Specifically, CYP2D6 is primarily expressed in the liver. It is also highly expressed in areas of the central nervous system, including the substantia nigra.
	CYP3A4 Inhibition	The CYP P450 genes are involved in the formation and breakdown (metabolism) of various molecules and chemicals within cells. Specifically, CYP3A4 is an important enzyme in the body, mainly found in the liver and in the intestine. It oxidizes small foreign organic molecules (xenobiotics), such as toxins or drugs, so that they can be removed from the body.
	CYP2C9 Inhibition	The CYP P450 genes are involved in the formation and breakdown (metabolism) of various molecules and chemicals within cells. Specifically, the CYP P450 2C9 plays a major role in the oxidation of both xenobiotic and endogenous compounds.
	CYP2D6 Substrate	The CYP P450 genes are involved in the formation and breakdown (metabolism) of various molecules and chemicals within cells. Specifically, CYP2D6 is primarily expressed in the liver. It is also highly expressed in areas of the central nervous system, including the substantia nigra. Substrates are drugs that are metabolized by the enzyme.
	CYP3A4 Substrate	The CYP P450 genes are involved in the formation and breakdown (metabolism) of various molecules and chemicals within cells. Specifically, CYP3A4 is an important enzyme in the body, mainly found in the liver and in the intestine. It oxidizes small foreign organic molecules (xenobiotics), such as toxins or drugs, so that they can be removed from the body. Substrates are drugs that are metabolized by the enzyme.
	CYP2C9 Substrate	The CYP P450 genes are involved in the formation and breakdown (metabolism) of various molecules and chemicals within cells. Specifically, the CYP P450 2C9 plays a major role in the oxidation of both xenobiotic and endogenous compounds. Substrates are drugs that are metabolized by the enzyme.
Excretion	Half Life	Half life of a drug is the duration for the concentration of the drug in the body to be reduced by half. It measures the duration of actions of a drug.
	Clearance Microsome	Drug clearance is defined as the volume of plasma cleared of a drug over a specified time period and it measures the rate at which the active drug is removed from the body.
	Clearance Hepatocyte	Drug clearance is defined as the volume of plasma cleared of a drug over a specified time period and it measures the rate at which the active drug is removed from the body.
Toxicity	hERG	Human ether-à-go-go related gene (hERG) is crucial for the coordination of the heart's beating. Thus, if a drug blocks the hERG, it could lead to severe adverse effects. Therefore, reliable prediction of hERG liability in the early stages of drug design is quite important to reduce the risk of cardiotoxicity-related attritions in the later development stages.
	Ames Mutagenicity	Mutagenicity means the ability of a drug to induce genetic alterations. Drugs that can cause damage to the DNA can result in cell death or other severe adverse effects. Nowadays, the most widely used assay for testing the mutagenicity of compounds is the Ames experiment which was invented by a professor named Ames. The Ames test is a short-term bacterial reverse mutation assay detecting a large number of compounds which can induce genetic damage and frameshift mutations.
	DILI	Drug-induced liver injury (DILI) is fatal liver disease caused by drugs and it has been the single most frequent cause of safety-related drug marketing withdrawals for the past 50 years (e.g. iproniazid, ticrynafen, benoxaprofen).
	LD50	Acute toxicity LD50 measures the most conservative dose that can lead to lethal adverse effects. The lower the dose, the more lethal of a drug.